Conductance, I-V curves, and negative differential resistance of carbon atomic wires

Brian Larade, Jeremy Taylor,* H. Mehrez, and Hong Guo
Center for the Physics of Materials and Department of Physics, McGill University, Montreal, PQ, Canada H3A 2T8
(Received 18 December 2000; revised manuscript received 12 March 2001; published 31 July 2001)

We report on a first-principles analysis of transport properties of carbon atomic wires in contact with two metallic electrodes under external bias. The equilibrium conductance of the atomic wires is found to be sensitive to two factors: charge transfer doping, which aligns the Fermi level of the electrodes to the lowest unoccupied molecular orbital (LUMO) of the carbon chain, and the overlapping of scattering states to the LUMO. The conductance is also affected by the crystalline orientation of the electrodes. The low-bias current-voltage (I-V) characteristic is linear, but a negative differential resistance is observed at higher bias due to a shift of conduction channels relative to the states of the electrodes by the external bias potential. Our first-principles results give a clear physical picture of the molecule-electrode coupling, which is the controlling factor of electric conduction through the carbon atomic wires.

DOI: 10.1103/PhysRevB.64.075420 PACS number(s): 73.40.Cg, 73.40.Jn, 73.61.Ph, 73.40.Gk

I. INTRODUCTION

Quantum transport properties of atomic scale conductors have received great attention[1–14] recently because they represent the ultimate size limit of functional electronic devices. In many instances, the atomic scale systems demonstrated highly nonlinear current-voltage (I-V) characteristics, and therefore they have profound potential for device application. These interesting and important nonlinear properties include negative differential resistance and electromechanic and electrostatic current switching.[1–4,7,9] Experimental fabrication of atomic wires has progressed along several lines. Using the atomic manipulation ability of scanning tunneling microscopes (STM) or atomic force microscopes, an atomic wire can be formed between a sharp tip and a substrate and its electrical properties measured.[10,8,15,16] The atomic wires formed this way can be extremely small, involving only a few and even just a single atom.[8] A related experimental method for fabricating and investigating atomic wires is the break-junction technique,[17–19] where a metal filament under investigation is broken by a bending beam underneath. Further bending is then controlled by a piezovoltage, allowing fine adjustment of the distances of the two metal pieces in contact, forming an atomic wire in between. In addition to these clever mechanical techniques, substantial effort has been devoted to the fabrication of free-standing atomic wires using a variety of methods. For instance, several processes based on lithographic techniques have fabricated silicon or polycrystalline Si nanowires[20–23] with sizes in the few-nanometer range.

There has also been intense theoretical investigation of transport properties of atomic wires, using phenomenological, semiclassical, or quantum mechanical first-principles methods. So far, theoretical investigations have been focused on evaluating equilibrium conductance of atomic wires as a function of a control parameter such as the scattering electron energy or a geometrical parameter of the wires. A more important problem, clearly, is the prediction of current-voltage (I-V) characteristics for atomic wires because I-V curves are directly measured in an experiment and they contain the full nonlinear transport information not accessible by linear response transport coefficients. It is the purpose of this paper to report a first-principles investigation on the linear as well as nonlinear quantum transport properties of carbon atomic wires.

There have been several theoretical methods for analyzing transport properties of atomic scale conductors. The simplest approach is to estimate the shape of an atomic wire using physically plausible arguments, then assuming a hard wall potential for electron scattering, and finally obtain transmission coefficients.[24–28] For certain situations a qualitatively reasonable physical picture can be achieved using this simple approach on equilibrium conductance of a wire. At a more microscopic level, many authors apply semiempirical methods based on parametrized Hamiltonians, such as tight-binding or extended Hückel models, to investigate atomic wires.[29–37] The parametrized Hamiltonians are generally derived from the bulk or from isolated molecular systems; therefore the parameters usually do not account for such physical factors as the external bias and gate potentials. Finally, a more fundamental analysis is from first principles where the Hamiltonian of the system, including the atomic orbitals, the exchange-correlation interactions, the core-valence interactions, the coupling to the electrodes, as well as the effects of external fields, is calculated self-consistently without any phenomenological parameters.[38–52] However, first-principles analysis of the full I-V characteristics of atomic scale conductors is a difficult problem to solve. Indeed, despite the extensive literature on atomic wires, many of their most basic properties are still not well understood.

To further understand the electric conduction mechanisms at the atomic and molecular scale, in this work we report a detailed first-principles analysis of the I-V characteristics of carbon atomic wires. Carbon atomic wires are interesting conductors and have attracted considerable recent attention.[41,43] In particular, due to charge transfer doping[43] to the carbon atoms from the electrodes, the equilibrium conductance of short carbon wires varies with its length in a semi-periodic fashion.[41] Such behavior is neither Ohmic nor ballistic and therefore represents an interesting conduction behavior totally due to the atomic nature of the carbon valency. Comparing with previous work[41,43] on carbon atomic

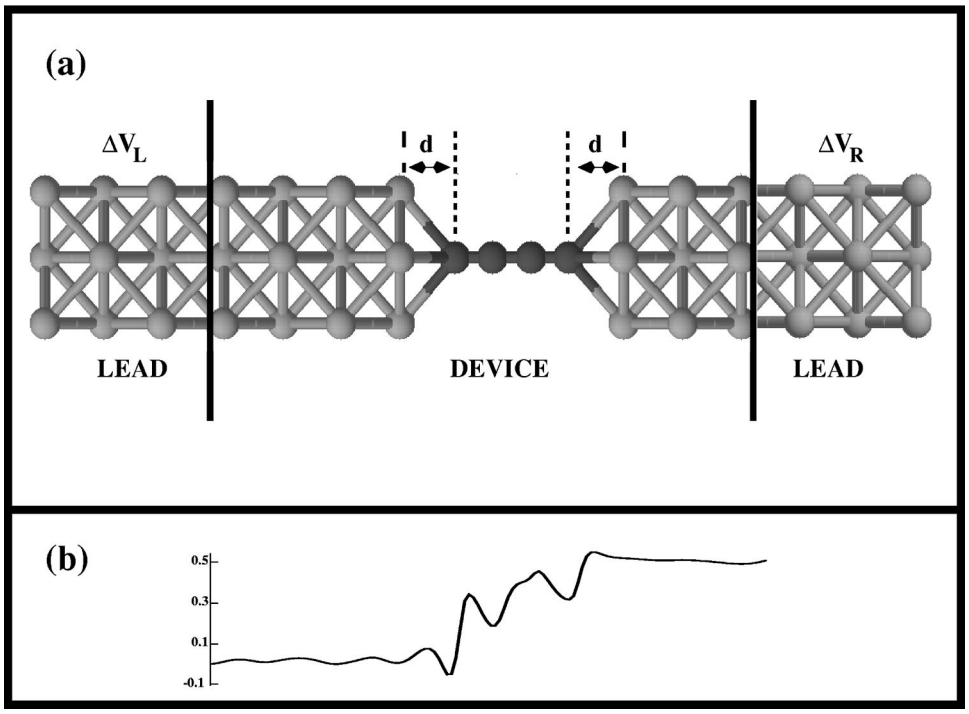

FIG. 1. (a) Schematic illustration of a carbon atomic wire. The wire consists of a short carbon chain in contact with two atomic scale Al electrodes. The chain-electrode contact distance is *d*. The electrodes extend to reservoirs at $z=\pm\infty$ where electric current is collected. The center box is the device scattering region which is included in our nonequilibrium Green's-function-based DFT analysis with the correct transport boundary conditions at the region boundaries. The external bias potential $\Delta V_{l/r}$ is applied to the left and right reservoirs. (b) Sample *X*-*Y* slice through the central cell showing how the Hartree potential V_H varies along the length of our device for an applied bias $\Delta V = 0.50$ eV.

wires, our focus is on two very important aspects not studied before: (1) What is the behavior of the *I*-*V* curves of carbon atomic wires? What are the physical factors that determine these behaviors? (2) What are the effects of atomic electrodes that connect to the carbon atomic wires? Previous investigations[41,43] on these wires used jellium electrodes; therefore any effects due to the crystalline structure of the electrodes were neglected. We will also report other results such as the behavior of equilibrium (at zero bias) conductance versus the carbon-wire–electrode distance, the charge transfer doping, and the conductance at a finite bias, for wires with atomic electrodes (as opposed to jellium electrodes).

Our results, obtained from first principles, clearly suggest that carbon atomic wires have nonlinear *I*-*V* characteristics if the electrodes are at atomic scale, and they display a negative differential resistance (NDR) behavior at high bias. This is a very interesting result because NDR is typically observed in semiconductor devices in the resonant tunneling regime, which is a very different situation as compared with the very conductive carbon atomic wires. NDR has also been observed in STM measurements involving a tip and a substrate separated by a vacuum tunneling barrier.[53,7] There, the NDR is understood as due to the on-and-off alignment of narrow features in the density of states (DOS) of the two parts (tip and substrate) across the tunnel junction. For the conductive carbon atomic wire and its NDR, this DOS picture turns out to be quite helpful. By a combined consideration of the DOS effects of the two atomic electrodes with the electronic properties of the carbon wires, the NDR can be well understood. We have investigated the equilibrium conductance of short carbon atomic wires with odd and even numbers of carbon atoms, and found that the conductance oscillates with the carbon-atom–electrode contact distance. This behavior is a direct consequence of two physical factors: the charge transfer doping effect, which aligns the Fermi level of the electrodes to the LUMO state of the isolated carbon chain, and the overlapping of the scattering states of the wire to LUMO states. The equilibrium conductance is also found to be sensitive to the crystalline orientation of the atomic electrodes. Our first-principles results give a clear physical picture on the molecule-electrode coupling, which is the controlling factor of electric conduction through the carbon atomic wires.

The paper is organized in the following way. In the next section we briefly outline our model of the atomic wire, and the theoretical and computational technique used in our analysis; Sec. III presents our results on the *I*-*V* curves and Sec. IV on the behavior of zero-bias conductance; a short summary is contained in Sec. V.

II. SYSTEM AND METHOD

In order to predict quantum transport properties of atomic scale conductors, especially the *I*-*V* curves, we have developed a modeling technique within the first-principles density functional theory[54–56] (DFT) approach. The details of this technique are presented elsewhere,[57,58] and in this section we briefly outline the main points for completeness of the presentation.

We consider carbon atomic wires shown in Fig. 1(a), where a short chain of carbon atoms are in contact with two Al atomic electrodes that extend to electron reservoirs at $z=\pm\infty$ where the electric current is collected. We investigate wires with different lengths as a function of bias potential and the chain-electrode contact distance *d*. We investigate the consequences of atomic scale electrodes, specifically Al electrodes with a finite cross section oriented in the [100] or [111] direction. In the calculation we have fixed the atomic positions of both the electrodes and wire. The (100) electrode

is represented by a slab of Al atoms oriented along the (100) plane with 18 atoms per unit cell repeated to $z=\pm\infty$. For the (111) electrodes, each repeating unit cell contains 32 atoms. The carbon atoms making up our wire are separated by 2.5 a.u.[59,41] The carbon atoms in contact with the electrodes are positioned at the hollow site for Al(100) electrodes and at the top site for the Al(111) electrodes.

When an external bias potential $\Delta V_{l/r}$ is applied to the left (l) and to the right (r) reservoirs, the electrochemical potentials, $\mu_{l/r}+\Delta V_{l/r}$, of the two electrodes are not equal and the atomic wire is in a nonequilibrium steady state. Here $\mu_{l/r}$ is the chemical potential of the reservoirs. We also note that the conductor in Fig. 1(a) is an *open* system and is therefore infinitely large due to the presence of electrodes. This is in clear contrast to the familiar situations normally analyzed in DFT that are either finite (as in quantum chemistry) or consist of periodic supercells (as in solid-state physics). In order to deal with the open structure and the nonequilibrium situation from first principles, we proceed as follows.[57,58]

First, we reduce the infinitely large *open* conductor to something numerically tractable by making a simple observation that the Kohn-Sham potential $V_c^{\rm eff}(\mathbf{r})$ deep inside an electrode surface (i.e., far away from the carbon atoms) is very close to the corresponding bulk Kohn-Sham potential. This bulk potential is calculated within DFT and stored into an electrode database for later use. To analyze the device, we divide it into three sections: the left and right electrodes, and the central cell, which is actually our DFT simulation box [see Fig. 1(a)]. Note that the central cell contains a portion of the electrodes [Fig. 1(a)] and all the atoms inside the central cell are included in our DFT self-consistent iterations. During the iteration, we require that at the boundary of the central cell, the potential $V_c^{\rm eff}(\mathbf{r})$ is matched with that of the corresponding bulk Kohn-Sham potential of perfect electrodes stored in our electrode database. The external bias potential is then easily applied as the boundary condition for the Hartree potential, which we solve in real space using a multigrid numerical technique.[57,58] As an example, Fig. 1(b) plots the calculated Hartree potential at bias $\Delta V=+0.5$ V minus its value at $\Delta V=0$, across the atomic wire at a given transverse position. In our calculations we varied the size of the central cell (the length of the electrodes included there) until no change is detected in the physical quantities.

Second, in order to carry out the DFT analysis, one must calculate the charge distribution $\rho(\mathbf{r})$ for the system. In conventional DFT self-consistent iterations, $\rho(\mathbf{r})$ is constructed by summing over the Kohn-Sham eigenstates. For an open conductor such as that of Fig. 1(a), while one can determine all the scattering states that connect $z=-\infty$ to $z=+\infty$ across the carbon chain, it is very difficult to determine all the bound states that exist inside the scattering region.[57,58] The reason that there may be bound states is because the bandwidth of the carbon chain can be larger than that of the electrodes; therefore the chain region behaves as a potential well. To overcome this difficulty, and indeed, to deal with the nonequilibrium condition due to external bias, we construct $\rho(\mathbf{r})$ using the Keldysh nonequilibrium Green's function[60–62] $G^<$,

$$\hat{\rho}=-\frac{i}{2\pi}\int dE\, G^<(E), \tag{1}$$

where, within a one-particle theory such as the DFT,

$$G^<=G^R\Sigma^<[f^{k_l^n},f^{k_r^n}]G^A. \tag{2}$$

Here $G^{R/A}$ is the retarded/advanced Green's function of the conductor. The quantity $\Sigma^<[f^{k_l^n},f^{k_r^n}]$ represents injection of charge from the electrodes[61] and can be written in terms of the self-energies $\Sigma^l_{l,l}$ and $\Sigma^r_{r,r}$ due to coupling to the left and right electrodes,

$$\Sigma^<[f^{k_l^n},f^{k_r^n}]=-2i\,\mathrm{Im}(f^{k_l^n}\Sigma^l_{l,l}+f^{k_r^n}\Sigma^r_{r,r}), \tag{3}$$

where $f^{k_l^n}$ and $f^{k_r^n}$ are the Fermi distributions of the left and right electron reservoirs. The charge density constructed this way, including both scattering states and bound states, together with the boundary condition discussed above, is the correct density for open systems under external bias. Using the boundary conditions on the effective potential mentioned above and given the distribution functions $f^{k_l^n},f^{k_r^n}$, the method we have developed[57,58] yields the *exact* solution to the Kohn-Sham equations as the size of the simulation cell increases.

In this work we use a minimal s,p real space fireball linear combination of atomic orbitals (LCAO) basis set,[57,58,63] and use the standard nonlocal norm-conserving pseudopotential[64] to define the atomic cores. In this way the Hamiltonian of the wires can be organized into a tridiagonal form and the Green's functions G^R,G^A can be obtained by direct matrix inversion in the orbital space.[57,58] The use of a minimal basis set results in an efficient calculation and also acceptable accuracy as amply documented in the literature.[57,58,46,65,63,66] Finally, we calculated the self-energies $\Sigma^l_{l,l}$ and $\Sigma^r_{r,r}$ by extending[57,58] a technique discussed in Ref. 67.

Once $\rho(\mathbf{r})$ is obtained, we evaluate all other relevant terms in the effective potential $V_c^{\rm eff}(\mathbf{r})$ including the exchange-correlation and the core contributions. In this way we iterate the self-consistent Kohn-Sham equation to numerical convergence, which we choose as 10^{-4} eV for the band-structure energy. Physical quantities are then collected, and in particular we obtain electric current by evaluating the Landauer formula,

$$I=\frac{2e}{h}\int_{\mu_{\min}}^{\mu_{\max}}dE(f^{k_l^n}-f^{k_r^n})T(E,\Delta V), \tag{4}$$

where $T(E,\Delta V)$ is the transmission coefficient at energy E and bias potential ΔV, given by[60]

$$T(E,\Delta V)=4\,\mathrm{Tr}[\mathrm{Im}(\Sigma^l_{l,l})G^R_{l,r}\,\mathrm{Im}(\Sigma^r_{r,r})G^A_{r,l}]. \tag{5}$$

It is emphasized that, since the current is calculated from a self-consistent analysis, the functions inside the trace in Eq. (5) are all functions of bias potentials $\Delta V=(\Delta V_r-\Delta V_l)$.

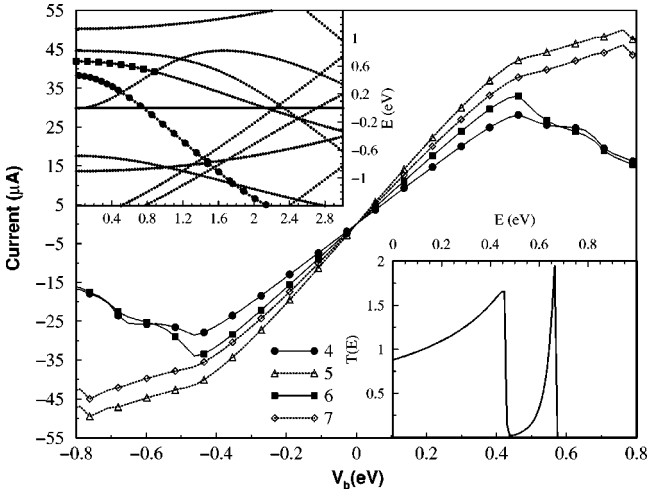

FIG. 2. The current-voltage characteristics of the Al(100)-C_N-Al(100) carbon atomic wires including $N=4\rightarrow7$ carbon atoms. The contact distance is fixed at $d=1.90$ Å . Upper inset: band structure $E=E(k)$ of the atomic electrodes with k along the wire direction (z axis). The Fermi level of the electrodes is at $E_F=0$, shown as the horizontal solid line, which cuts several possible bands at various k. For a given energy E, not all electrode Bloch states contribute to conduction. There are two bands (each degenerate), indicated by the solid circles and squares, which contribute to transmission through the carbon wires. Lower inset: the transmission coefficient $T(E)$ versus electron energy E for the Al(100)-C_4-Al(100) wire at zero bias. The two conducting states of the electrodes are responsible for the two ''peaks'' in the transmission.

III. THE *I-V* CHARACTERISTICS

Figure 2 presents the typical I-V curves of the atomic wires with 4–7 carbon atoms in contact with two Al(100) electrodes. The carbon atom in contact with an electrode is positioned at the hollow site of the (100) electrode slab, with the carbon-atom–electrode distance chosen as $d=1.90$ Å . Several observations are in order. First, all the wires display metallic I-V characteristics, with a linear region between -0.46 V and $+0.46$ V. In this linear regime, the slope of the I-V curves, dI/dV, gives the equilibrium conductance G of the wires. In unit of $G_o\equiv 2e^2/h$, G can also be directly calculated from Eq. (5), $G=T(\mu)$. Second, nonlinearity sets in at a higher bias $\sim\pm0.5$ V for all the wires. Third, for wires with even number of carbon atoms (4 and 6), a negative differential resistance is observed at around ±0.46 V, where the current decreases with increasing bias voltage. Finally, NDR is also observed for chains with an odd number of carbon atoms (5 and 7), but at another (higher) bias as shown in the figure. For these odd-number chains, current keeps increasing after nonlinearity sets in, but with a slower gradient. It is extremely surprising that an atomic wire can have NDR nonlinearity. For simple wires one would expect a linear I-V curve plus, at most, a current saturation at large bias. The fact that current goes down with an increasing bias for a good conducting atomic wire needs further analysis.

For the familiar double barrier resonant tunneling diodes fabricated using semiconductor heterostructures,[68] NDR is due to shifting of the resonance state inside the tunnel barriers by the bias potential. At small bias, the resonance state is higher than the Fermi level of the electrode; therefore transport is off-resonance leading to a small current. At a larger bias, the resonance level is pushed down to align with the Fermi level of the source electrode leading to resonant tunneling, and a larger current flows. At even larger bias, the resonance level is pushed below the edge of the conduction band of the semiconducting source electrode, giving rise to a drop in the tunneling current. This gives the familiar NDR of resonant tunneling diodes.[68] This physical picture of NDR, however, does not apply to our atomic wires because the wires are not in the tunneling regime and because the electrodes are metallic.

Another interesting scenario that is very useful to our situation is the NDR discussed in the STM literature.[53] In an STM experiment, if the tip is in the atomic scale, narrow features in the density of states can develop at the tip apex. When the tip is near the sample surface being studied, the narrow tip DOS feature can be tuned to align with localized states of the sample by the bias potential. Therefore, the tunneling current is low at small bias before the alignment; at a larger bias when alignment occurs the current becomes high; and it becomes low again at even higher bias when the DOS feature of the tip is off alignment. This gives NDR, as observed in Ref. 53, in either the positive-bias or the negative-bias side of the I-V curve. Recently this physical picture was extended to understand the NDR observed in STM experiments on organic molecules[7] where NDR was observed in both bias polarities. For the atomic wires considered here, although conduction is not in the tunneling regime as are the STM experiments where narrow DOS features of the tip and of the sample can be defined relatively unambiguously, we found the STM physical picture[53,7] to be quite helpful in understanding the NDR of the atomic wires.

To understand the origin of NDR, in the upper inset of Fig. 2 we plot the band structure of a perfect periodic Al electrode, and there are several bands crossing at the Fermi level $E_F=\mu=0$ indicated by the horizontal line (the Fermi level of the infinitely long electrode is shifted to zero energy). These bands are the possible incoming states for electron transport at E_F. In fact, for any energy E there are several possible incoming states, but not all contribute appreciable transmission through the atomic wire. For the atomic wires studied here, we found that there are two scattering states, each *doubly degenerate*, which connect $z=-\infty$ to $z=+\infty$ across the carbon chain. We obtained these scattering states $\Psi^{k_l^n}(E)$ using our *ab initio* technique.[57,58,33] Here E is energy of the incident electron and the superscript k_l^n labels the scattering states incident from the left lead. These two scattering states correspond to the bands plotted as circles and squares in the upper inset of Fig. 2. We shall refer to these two bands as ''significant electrode bands'' because they contribute most significantly to conduction. In the lower inset of Fig. 2 we plot the total transmission coefficient $T(E)$ versus energy E at zero bias for the Al(100)-C_4-Al(100) wire. At $E\approx0.46$ eV, which is the band edge of the lower significant electrode band (the circles in the band structure

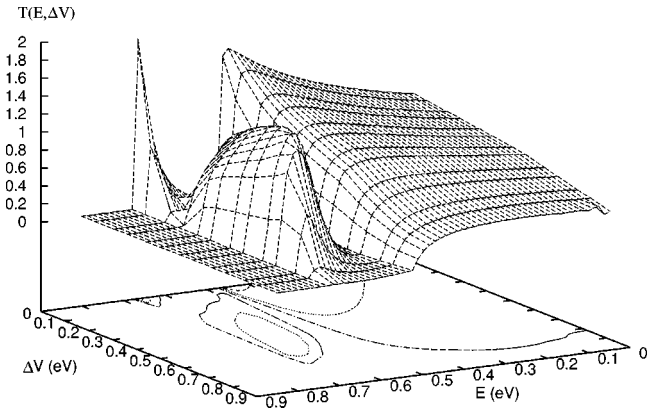

FIG. 3. The transmission coefficient $T=T(E,\Delta V)$ for the Al(100)-C_4-Al(100) carbon atomic wire.

inset), $T(E)$ drops to very small values as expected. $T(E)$ then increases gradually due to the participation of the second significant electrode band (the squares in the band structure inset) until $E\approx 0.65$ eV, which is its band edge. After that $T(E)$ is essentially zero because none of the other electrode bands can transmit through the carbon wire.

Clearly, $T(E)$ is a function of bias voltage as well. In Fig. 3 the complete behavior of $T=T(E,\Delta V)$ is plotted against E and ΔV for the Al(100)-C_4-Al(100) carbon wire. In general, fixing ΔV, $T(E,\Delta V)$ increases with E until the band edge at 0.46 eV, where it sharply drops to small values. Increasing E further, the second significant electrode band starts to play a role and $T(E,\Delta V)$ increases, leading to a ''hump'' at larger E. On the other hand, for a fixed energy E, $T(E,\Delta V)$ decreases slowly and monotonically with ΔV for $E<0.46$ eV, and shows two humps for $E>0.046$ eV. It is easy to understand that these two humps are results of the two significant electrode bands: at $\Delta V=0$ we see a sharp peak due to the matching of the upper significant electrode bands in the left and right electrodes. As ΔV is increased, the bands of the *right* electrode will be shifted up and we initially see the dip corresponding to the movement of the gap between the upper and lower significant electrode bands into our energy range, followed by a broad hump due to the lower significant band.

The increasing part of the *I-V* curve, between ± 0.46 eV, can now be easily understood. As the bias is increased (or decreased), the relative position of the band structure of the left and right electrodes is shifted apart by the bias. Throughout our calculations we have fixed $V_l=0$ and varied $V_r=\Delta V$. Since there is a significant electrode band between $E_F=0$ and $E\approx 0.46$ eV (the circles of the upper insert of Fig. 2), as ΔV increases from zero to 0.46 eV the current increases because more and more conduction density of states are included into the integration window below $\mu_{\max}=E_F+e\Delta V$ [see Eq. (4)], despite the slow decrease of $T(E,\Delta V)$ as a function of ΔV (see Fig. 3). However, when ΔV reaches 0.46 eV there are no additional conduction density of states for the left electrode (see upper inset of Fig. 2). Therefore, we expect a change of behavior of the current when ΔV reaches 0.46 eV. Indeed, we observe a decrease of current for carbon wires with even numbers of atoms, and a slower increase of current for those with odd numbers of carbon atoms.

Immediately after $\Delta V=0.46$ eV, the behavior of the *I-V* curve must be due to the carbon atoms themselves because the left electrode has no more bands to offer significant conduction. To check this, we have calculated the electronic states of *isolated* carbon chains with 4–7 atoms, denoting them as Φ_i^c. Projection of $\Psi^{k_l^n}(E)$ onto Φ_i^c gives us a measure of which ''molecular state'' is more important for conduction. Our data showed that while many carbon eigenstates contribute to conduction, the LUMO state is the most important and it carries over 90% of the weight on the projection coefficient,

$$P_i \equiv |\langle \Phi_i^c | \Psi^{k_l^n}(E)\rangle|^2 \tag{6}$$

for all energies we have checked. Due to this fact (which will be further discussed in the next section), let us focus on the LUMO projection P_{LUMO}. It is important to note that the LUMO state we define is not that of the isolated molecule, rather it is the new lowest unoccupied state that arises from the transfer of charge from the electrodes to the carbon wire.[71]

Why does the current start to decrease at $\Delta V\approx 0.46$ eV for even-atom carbon wires? This is because, for these wires, the coupling of the LUMO state of the carbon chain to the electrodes becomes worse as ΔV is increased. Consider Fig. 4(a), which shows the transmission spectrum of the Al(100)-C_4-Al(100) wire for three different values of ΔV. Upon examination of the energy level structure of the C_4 chain (and other chains), the data show a good one-to-one correspondence between the peaks in the transmission coefficients and the molecular orbitals of the chain.[69] Therefore transmission is dominated by a resonance behavior through the molecular orbitals. At zero bias, for the even chain [i.e., C_4, Fig. 4(a)] the LUMO position, indicated by the inverse triangle, is above $E_F=0$ (E_f fixed by the electrodes). When a positive bias is applied, the even-chain LUMO transmission peak shifts to higher energy further away from E_F, in addition to a change in the shape of transmission coefficient $T(E,\Delta V)$, indicating an increasing ΔV leads to a weaker coupling between the LUMO and the electrode states. This is the reason that the coefficient P_{LUMO}, shown as the inset to Fig. 4(a), decreases in the entire range of ΔV for all the energies of the even chain, indicating that the nonequilibrium condition provided by a finite ΔV reduces the interaction between the LUMO and the electrode states. Before ΔV reaches ~ 0.46 eV, the decreasing of P_{LUMO} by an increasing ΔV is more than compensated by the fact that more scattering density of states are included into the window $\mu_{\max}=E_F+\Delta V$ as discussed above, and current therefore increases with ΔV. But immediately after $\Delta V\approx 0.46$ eV, the left electrode has no more bands to offer significant conduction, as a result the decreasing P_{LUMO} becomes the dominant factor, giving rise to the reduction of current. When ΔV further increases to ~ 0.6 eV, the second significant electrode band of the left electrode (squares of upper inset of Fig. 2) starts to contribute which partially compensates the decrease of P_{LUMO}. As a result, the current shows a small structure at

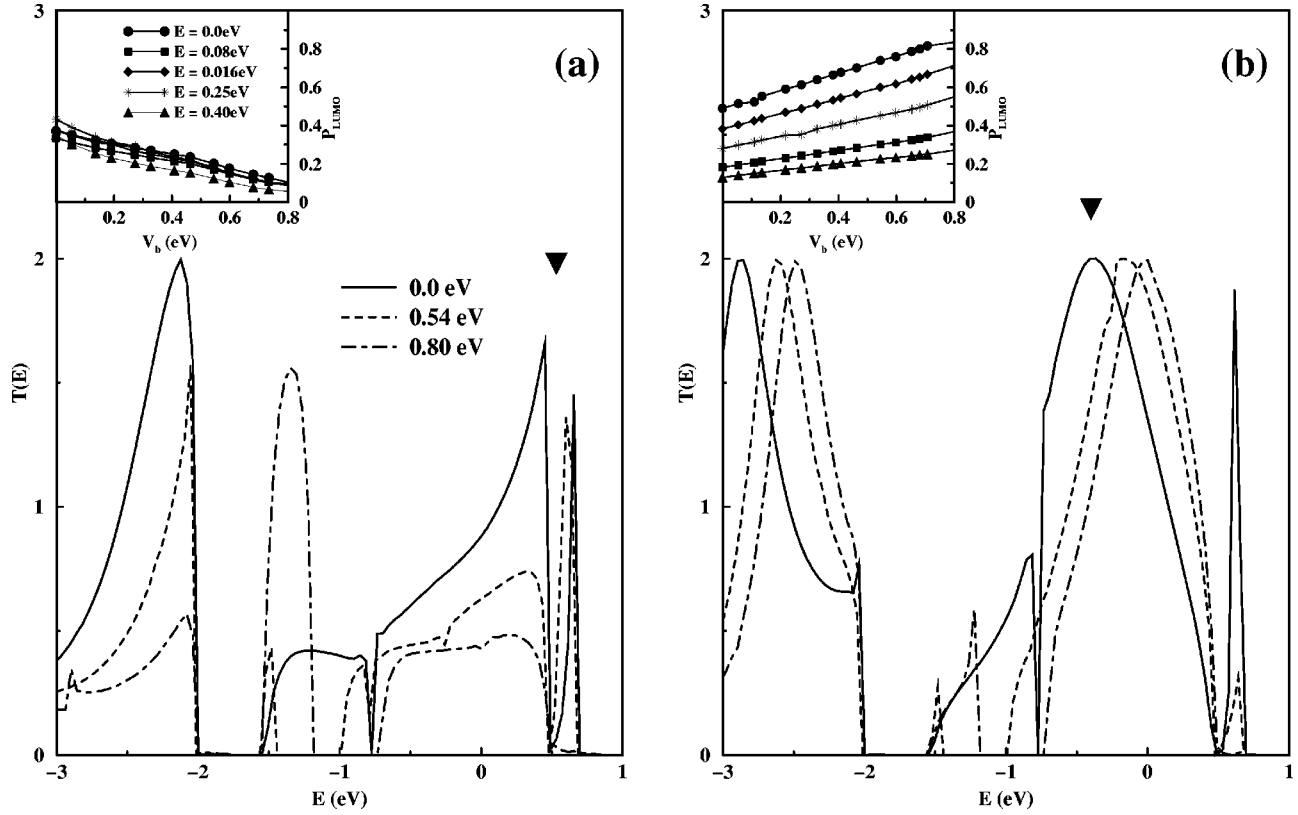

FIG. 4. The transmission spectrum of the carbon atomic wires for different bias potentials V_b. The arrow indicates the peak corresponding to the LUMO state of the carbon chain. (a) $T(E)$ for C_4; (b) $T(E)$ for C_5; insets: The projection (arbitrary units) of the scattering states onto the charge-transferred, ''new'' LUMO of the isolated carbon chain, as a function of bias potential V_b, for a number of electron energies E ranging from $E=0$ to 0.4 eV. (a) Projection onto C_4 LUMO; (b) projection onto C_5 LUMO.

$\sim$0.65 eV. We have checked that the same behavior occurs for the six-atom carbon wire. Therefore, the NDR in the even-atom chains is due to the coupling dependence of the carbon-chain LUMO state to the electrodes as a function of ΔV.

We have carried out exactly the same analysis for the odd-chain wires. For an Al(100)-C_5-Al(100) wire, Fig. 4(b) plots its transmission as a function of energy, and the inset plots its P_{LUMO} versus bias ΔV. For odd chains the LUMO is below E_F at zero bias, and a positive ΔV moves it toward and eventually across E_F, resulting in an improved coupling between the LUMO and the electrode states as ΔV is increased. Indeed, the inset of Fig. 4(b) shows P_{LUMO} to increase with ΔV for the entire range, exactly opposite to the behavior of even-chain wires. Therefore, the current should continue to increase past the electrode band edge when $\Delta V \approx 0.46$ eV. This is indeed the observation of the I-V curves in Fig. 2.

We can therefore conclude that the nonlinear I-V curves of the carbon atom wires studied here, especially the NDR for the even-atom wires, are due to competition between how well the carbon-chain LUMO states couple to the atomic scale electrodes and how much scattering density of states contribute to the current [through Eq. (4)], as a function of the bias potential ΔV. Because of the role played by the discrete electrode band structure, to observe the NDR it is essential that the electrodes immediately in contact with the carbon chain have small cross sections. It is also quite surprising that for a very conductive wire like ours, the behavior of the I-V curve can be understood reasonably well from the electronic structures of the parts: the band structure of the electrodes and the eigenstates of the carbon chains, if the scattering states of the wire Ψ^E are known. Finally, we have also investigated the I-V curves for cases of Al(111) electrodes, and a similar understanding has been obtained.

IV. THE CONDUCTANCE

The equilibrium conductance G has been analyzed previously for carbon chains in contact with jellium electrodes.[41,43] In this section we present results of G for wires with atomic electrodes.

For a fixed carbon-chain–electrode distance $d=1.90$ Å, Fig. 3 shows how G varies with electron energy and with bias potential ΔV. Figures 5(a) and 5(b) plot G as a function of d for wires with 4–7 carbon atoms for Al(100) and Al(111) electrodes, respectively. The most striking feature is the oscillatory behavior as d is increased.[70] This behavior was also observed in the jellium-C_5-jellium wire.[41] Another interesting feature is that the curves of even-atom wires follow each other, while those of odd-atom wires also follow each other. For the Al(100) electrodes, the conductance of the odd- and even-atom wires oscillate almost exactly ''out of phase'' [see Fig. 5(a)]. We clearly expect G to vary with

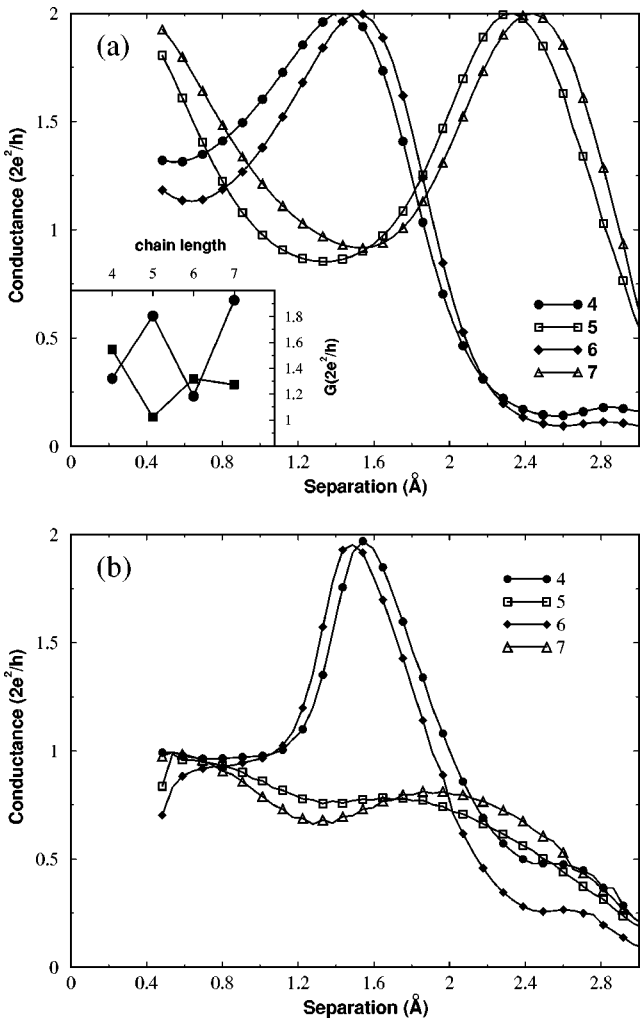

FIG. 5. The conductance of the carbon atomic wires versus contact distance *d*. (a) For Al(100)-C_N-Al(100) wires; (b) for Al(111)-C_N-Al(111). The inset of (a) plots conductance versus the number of carbon atoms: circles are with $d=0.5$ Å, squares are with $d=0.95$ Å.

the contact distance *d*, but why in an oscillatory fashion?

We investigate this question and other behaviors of conduction by looking at how the individual states of an isolated carbon chain contribute to the total conductance, using the scattering states projection technique, with Al(100)-C_4-Al(100) wire as an example. An important feature of the molecule-electrode interaction is the charge transfer doping,[43] where charges transfer to the carbon chain from the metallic electrodes at equilibrium due to the electronegative nature of the carbon chains. Our calculation indicates that at small contact distance $d\approx 0.5$ Å [see Fig. 1(a)], two extra charges are transferred; while at larger distance $d\approx 2.5$ Å, one extra charge is transferred. We have also found that the total amount of transferred charge is a smooth decreasing function of *d*. As a comparison, for wires with jellium electrodes, Ref. 43 reported one extra charge is transferred to a C_4 chain. As discussed previously[43] and as our calculations show, charge transfer has the important consequence of doping the molecular orbitals of the carbon chain. For example, an isolated even-atom carbon chain such as C_4 has a partially filled highest occupied molecular orbital (HOMO). When attached to electrodes, charge transfer from the electrodes fills the HOMO and, depending on how much charge is transferred, can further partially fill the next highest level, which is LUMO. On the other hand, odd-atom carbon chains such as C_5 have a filled HOMO and empty LUMO, and charge transfer partially fills the empty LUMO. Clearly, these carbon-chain states are somewhat broadened when electrodes are attached, but the important consequence of charge transfer is the alignment of the LUMO (or HOMO) of the carbon chain to the Fermi level of the electrodes, and these states contribute most significantly to conduction.

For the Al(100)-C_4-Al(100) wire, we found that there are two scattering states (each is twofold degenerate) which contribute to the equilibrium conductance. Using Eq. (6), we projected these two scattering states, $\Psi^{k_l^n}(E)$, to all the molecular orbitals of the isolated C_4 chain, and found that the LUMO dominates with over 90% weight for all the contact distances *d*. Figures 6(a) and 6(b) plot the projection coefficients of the two scattering states onto the LUMO, together with the transmission coefficients of these two scattering states, as a function of *d*. It is observed that P_{LUMO} and $T(E_F)$ follow a very similar functional dependence on *d*, clearly demonstrating that the values of transmission $T(E_F)$ are directly controlled by how well the scattering states overlap with the LUMO. This overlapping, as shown by Fig. 6, is affected by the contact distance *d*. Similar conclusions can be drawn as we have confirmed, for odd-atom wires such as Al(100)-C_5-Al(100).

In Fig. 7(a), we plot the two transmission coefficients due to the two scattering states together, as a function of *d*. They add up (after taking into account the degeneracy) to give the total transmission (solid line). Clearly, one of the scattering states (solid triangles) contributes more prominently at lower values of *d*, while the other (solid circles) is

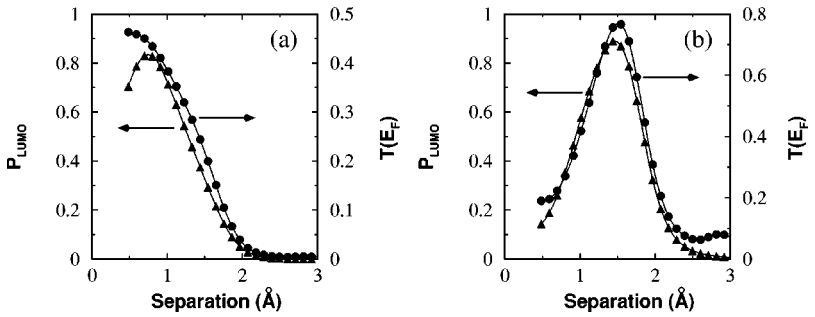

FIG. 6. Transmission coefficients (solid circles) of the two scattering states, and their projection (solid triangles) onto the LUMO of the isolated C_4 chain. (a) For the first scattering states; (b) for the second scattering states. The projection P_{LUMO} is plotted in arbitrary units.

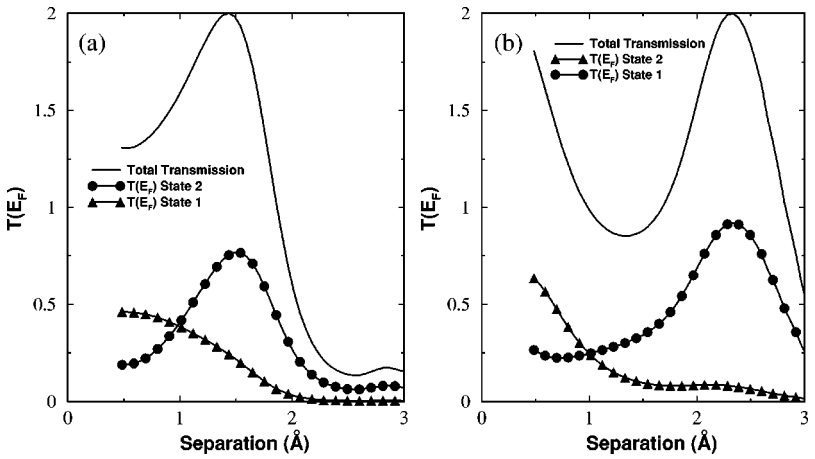

FIG. 7. Transmission coefficients of the two scattering states (solid circles and triangles, each doubly degenerate) and the total transmission (solid line), as functions of the contact distance *d*. (a) For Al(100)-C_4-Al(100) wire; (b) for Al(100)-C_5-Al(100) wire.

more important at larger *d*. This is a consequence of how well they overlap with the LUMO as discussed in the last paragraph. Therefore, when summed up, the total transmission or the conductance shows the oscillatory behavior shown in Fig. 5(a) for the Al(100)-C_4-Al(100) wire. We have confirmed that exactly the same happens for the odd-atom wires, shown in Fig. 7(b) using Al(100)-C_5-Al(100) as the example.

A previous investigation[41] on the jellium-C_N-jellium atomic wires observed a very interesting behavior: the equilibrium conductance *G* varies nonmonotonically with the number of carbon atoms. Such a behavior is also reported for Au wires as due to standing waves along the wire.[33] Our conductance curves in Fig. 5(a) also show this behavior for each fixed contact distance *d*. Since our electrodes are very different from the jellium electrodes, we have checked that our numerical values are closest to that reported in Ref. 41 at $d=0.5$ Å, which are shown as the solid circles in the inset of Fig. 5(a). At this distance, odd-atom wires have larger conductance than the even-atom wires. At a distance $d=0.95$ Å, shown as solid squares in the inset of Fig. 5(a), the even-atom wires have larger conductance. Clearly, from the behavior of the curves in Fig. 5(a), this odd-even property varies depending on the value of *d*. This is, once again, due to the coupling of the HOMO and LUMO to the electrodes, which varies with *d*. To test these results further, we have examined the difference between top site and hollow site binding of the carbon wires to the Al(100) electrodes. The results show that for $d<1.5$ Å, the different binding sites change the transport properties, which is not surprising. At larger separations the effect vanishes and quantitative agreement is obtained for different binding sites. This suggests that the crystalline structure of the electrodes plays a more important role than the binding site in determining how molecular orbitals of the carbon chain couple to the electrodes. Indeed, our results on the Al(111)-C_N-Al(111) wires, Fig. 5(b), show qualitatively similar but quantitatively very different oscillatory behavior.

V. SUMMARY

In this paper we have investigated quantum transport properties of carbon atomic wires in contact with atomic scale electrodes, using a first-principles technique that is based on density-functional theory and nonequilibrium Green's functions. We report the current-voltage characteristics for these wires, and found that the *I-V* curves can have a region of negative differential resistance. The reported NDR is due to a competition between how well the carbon-chain LUMO couples to the atomic scale electrodes, and how much scattering density of states contribute to the current, as a function of the bias potential. This mechanism is somewhat similar to that established in the atomic scale STM measurement in which NDR is a consequence of the narrow features in the density of states on the two sides of the tunnel junction.[53,7] We emphasize that for the carbon atomic wires, in order to observe NDR, narrow atomic scale electrodes are necessary. This presents an experimental challenge.

The transport properties of the carbon atomic wires depend on charge transfer from the electrodes. An isolated even chain has a partially filled degenerate HOMO. When contacted with electrodes, for example at $d=1.9$ Å, there is slightly more than one extra charge transferred from the electrodes to the chain, which causes a further filling of the HOMO. As a result the empty LUMO state of even chains lie above E_F [as seen in Fig. 4(a)]. The isolated odd chains, by comparison, has a filled HOMO, and after charge transfer acquires a partially filled LUMO, which will, as expected, lie below E_F [Fig. 4(b)]. It can clearly be seen that the role of charge transfer in aligning the LUMO state of the carbon chains to the electrodes cannot be underestimated.

We have provided a general picture of how the transmission coefficients vary with both scattering electron energy and bias voltage. More importantly we found that the equilibrium conductance of the wires show an odd-even ''parity'' in their oscillatory variation with the contact distance *d*. Our analysis showed that the oscillatory behavior is due to the overlap of scattering states with the LUMO states of the isolated carbon chain. Very interestingly, the main features of the conduction can be well understood by projecting the scattering states onto the molecular orbitals of the isolated carbon chain and by examining the electrode states. This provides a powerful theoretical method in analyzing conduction mechanisms of molecular scale systems. Our results further suggest that for carbon atomic wires the odd-even ''parity,'' namely odd chains behave similarly while even chains also

behave similarly, is more general than the one expected as this property is qualitatively insensitive to electrodes, be it Al(100), Al(111), or jellium models.[41] On the other hand, there are other results that are expected to be sensitive to details of the atomic wire structure, for instance, the precise bias voltage at which NDR occurs as it is related to electrode band structure. It is the hope of the authors that by examining various specific atomic/molecular scale conductors, a general physical picture can emerge on the conduction mechanisms and current-voltage characteristics of molecular electronics.

ACKNOWLEDGMENTS

We gratefully acknowledge financial support from NSERC of Canada and FCAR of Quebec (H.G); B.L. and J.T. gratefully acknowledge financial support from NSERC through PGS; H.M. gratefully acknowledges financial support by the Carl Reinhardt McGill Foundation.

*Present address: Mikroelektronik Centret (MIC), Technical University of Danmark, East DK-2800 Kgs. Lyngby, Denmark.

[1] C. P. Collier, G. Mattersteig, E. W. Wong, Y. Luo, K. Beverly, J. Sampaio, F. M. Raymo, J. F. Stoddart, and J. R. Heath, Science **285**, 391 (1999); **289**, 1172 (2000).

[2] M. A. Reed, C. Zhou, and C. J. Muller, Science **278**, 252 (1997); J. Chen, M. A. Reed, and A. M. Rawlett, *ibid.* **286**, 1550 (1999); J. Chen, W. Wang, M. A. Reed, A. M. Rawlett, D. W. Price, and J. M. Tour, Appl. Phys. Lett. **77**, 1224 (2000).

[3] C. Joachim, J. K. Gimzewski, R. R. Chlitter, and C. Chavy, Phys. Rev. Lett. **74**, 2102 (1995); J. K. Gimzewski and C. Joachim, Science **283**, 1683 (1999).

[4] T. Rueckes, K. Kim, E. Joselevich, G. Y. Tseng, C. Cheung, and C. M. Lieber, Science **289**, 94 (2000).

[5] S. J. Tans, M. H. Devoret, R. M. Alwin, and H. Dai, Nature (London) **386**, 474 (1997); S. J. Tans, J. Verschueren, R. M. Alwin, and C. Dekker, *ibid.* **393**, 49 (1998).

[6] J. W. G. Wildoeer, L. C. Venema, A. G. Rinzler, R. E. Smalley, and C. Dekker, Nature (London) **391**, 59 (1998).

[7] Y. Xue, S. Datta, S. Hong, R. Reifenberger, J. I. Henderson, and C. P. Kubiak, Phys. Rev. B **59**, 7852 (1999).

[8] A. Yazdani, D. M. Eigler, and N. Lang, Science **272**, 1921 (1996).

[9] C. Zhou, J. Kong, E. Yenilmez, and H. J. Dai, Science **290**, 1552 (2000).

[10] J. I. Pascual, J. Mendez, J. Gomez-Herrero, A. M. Baro, N. Garcia, U. Landman, W. D. Luedtke, E. N. Bogacheck, and H. P. Cheng, Science **267**, 1793 (1995); Phys. Rev. Lett. **71**, 1852 (1993).

[11] N. Garcia and L. Escapa, Appl. Phys. Lett. **54**, 1418 (1989).

[12] L. I. Glazman, G. B. Lesovik, D. E. Khmelnitskii, and R. I. Shekhter, Pis'ma Zh. Éksp. Teor. Fiz. **48**, 218 (1988) [JETP Lett. **48**, 238 (1988)].

[13] E. N. Bogachek, M. Jonson, R. I. Shekhter, and T. Swahn, Phys. Rev. B **47**, 16 635 (1993).

[14] M. Ogata and H. Fukuyama, Phys. Rev. Lett. **73**, 468 (1994).

[15] N. Agrait, J. G. Rodrigo, and S. Vieira, Phys. Rev. B **47**, 12 345 (1993).

[16] L. Olesen, E. Laegsgaard, I. Stensgaard, F. Besenbacher, J. Schiotz, P. Stoltze, K. W. Jacobsen, and J. K. Norskov, Phys. Rev. Lett. **72**, 2251 (1994).

[17] J. Moreland and P. K. Hansma, Rev. Sci. Instrum. **55**, 399 (1984).

[18] C. J. Muller, J. M. van Ruitenbeck, and L. J. de Jongh, Phys. Rev. Lett. **69**, 140 (1992).

[19] See, for example, E. Scheer, N. Agrait, J. C. Cuevas, A. Levy Yeyati, B. Ludoph, and A. Martin-Rode, Nature (London) **394**, 154 (1998), and references therein.

[20] H. Namatsu, Y. Takahashi, M. Nagase, and K. Murase, J. Vac. Sci. Technol. B **13**, 2166 (1995).

[21] Yasuo, Wada, T. Kure, T. Yoshimura, Y. Sudo, T. Kobayashi, Y. Goto, and S. Kondo, J. Vac. Sci. Technol. B **12**, 48 (1994); Jpn. J. Appl. Phys., Part 1 **33**, 905 (1994).

[22] Y. Nakajima, Y. Takahashi, S. Horiguchi, K. Iwadate, H. Namatsu, and K. Kurihara, Appl. Phys. Lett. **65**, 2833 (1994); Jpn. J. Appl. Phys., Part 1 **34**, 1309 (1995).

[23] H. I. Liu, D. K. Biegelsen, F. A. Ponce, N. M. Johnson, and R. F. W. Pease, Appl. Phys. Lett. **64**, 1383 (1994).

[24] E. Tekman and S. Ciraci, Phys. Rev. B **39**, 8772 (1989); **43**, 7145 (1991).

[25] M. Brandbyge, K. W. Jacobsen, and J. K. Norskov, Phys. Rev. B **55**, 2637 (1997).

[26] J. A. Torres, J. I. Pascual, and J. J. Sáenz, Phys. Rev. B **49**, 16 581 (1994); J. A. Torres and J. J. Sáenz, *ibid.* **54**, 13 448 (1996); Phys. Rev. Lett. **77**, 2245 (1996).

[27] J. L. Costa-Kramer, N. Garcia, P. Garcia-Mochales, and P. A. Serena, Surf. Sci. **342**, 1144 (1995).

[28] J. M. Krans, J. M. van Ruitenbeek, V. V. Fisun, I. K. Yanson, and L. J. De Jongh, Nature (London) **375**, 6534 (1995).

[29] P. L. Pernas, A. Martin-Rodero, and F. Flores, Phys. Rev. B **41**, R8553 (1990).

[30] W. Tian and S. Datta, Phys. Rev. B **49**, 5097 (1994).

[31] L. Chico, M. P. L. Sancho, and M. C. Munoz, Phys. Rev. Lett. **81**, 1278 (1998).

[32] A. L. V. de Parga, O. S. Hernan, R. Miranda, A. Levy Yeyati, N. Mingo, A. Martin-Rodero, and F. Flores, Phys. Rev. Lett. **80**, 357 (1998).

[33] E. G. Emberley and G. Kirczenow, Phys. Rev. B **60**, 6028 (1999).

[34] S. N. Yaliraki, M. Kemp, and M. A. Ratner, J. Am. Chem. Soc. **121**, 3428 (1999).

[35] M. Brandbyge, N. Kobayashi, and M. Tsukada, Phys. Rev. B **60**, 17 064 (1999).

[36] H. Mehrez, J. Taylor, H. Guo, J. Wang, and C. Roland, Phys. Rev. Lett. **84**, 2682 (2000).

[37] C. Roland, M. B. Nardelli, J. Wang, and H. Guo, Phys. Rev. Lett. **84**, 2921 (2000).

[38] N. D. Lang, Phys. Rev. B **52**, 5335 (1995).

[39] K. Hirose and M. Tsukada, Phys. Rev. B **51**, 5278 (1995).

[40] N. D. Lang, Phys. Rev. B **55**, 4113 (1997).

[41] N. D. Lang and Ph. Avouris, Phys. Rev. Lett. **81**, 3515 (1998).

[42] M. Di Ventra, S. T. Panetlides, and N. D. Lang, Phys. Rev. Lett. **84**, 979 (2000).

[43] N. D. Lang and Ph. Avouris, Phys. Rev. Lett. **84**, 358 (2000).

[44] C. C. Wan, J.-L. Mozos, G. Taraschi, J. Wang, and H. Guo, Appl. Phys. Lett. **71**, 419 (1997); C. C. Wan, J. L. Mozos, J. Wang, and H. Guo, Phys. Rev. B **55**, 13 393 (1997).

[45] J. Wang, H. Guo, J.-L. Mozos, C. C. Wan, G. Taraschi, and Q. Zheng, Phys. Rev. Lett. **80**, 4277 (1998).

[46] G. Taraschi, J.-L. Mozos, C. C. Wan, H. Guo, and J. Wang, Phys. Rev. B **58**, 13 138 (1998).

[47] J. L. Mozos, C. C. Wan, G. Taraschi, J. Wang, and H. Guo, Phys. Rev. B **56**, R4351 (1997); J.-L. Mozos, C. C. Wan, G. Taraschi, J. Wang, and H. Guo, J. Phys.: Condens. Matter **10**, 2663 (1998).

[48] J. Taylor, H. Guo, and J. Wang, in *Proceedings of the Fifth International Symposium on Quantum Confinement: Nanostructures, 194th Meeting of the Electrochemical Society*, edited by M. Cahay, D. J. Lockwood, J. P. Leburton, and S. Bandyopadhyay (The Electrochemical Society, Boston, 1998), p. 640.

[49] H. J. Choi and J. Ihm, Phys. Rev. B **59**, 2267 (1999).

[50] H. J. Choi, J. Ihm, Y. Y. Yoon, and S. G. Louie, Phys. Rev. B **60**, 14 009 (1999).

[51] H. J. Choi, J. Ihm, S. G. Louie, and M. L. Cohen, Phys. Rev. Lett. **84**, 2917 (2000).

[52] U. Landman, R. N. Barnett, A. G. Scherbakoy, and P. Avouris, Phys. Rev. Lett. **85**, 1958 (2000).

[53] In-Whan Lyo and Phaedon Avouris, Science **245**, 1369 (1989).

[54] P. Hohenberg and W. Kohn, Phys. Rev. **136**, 864 (1964).

[55] W. Kohn and L. J. Sham, Phys. Rev. **140**, 1133 (1965).

[56] R. G. Parr and W. Yang, *Density-Functional Theory of Atoms and Molecules* (Oxford University Press, New York, 1989).

[57] Jeremy Taylor, H. Guo, and J. Wang, Phys. Rev. B **63**, 121104 (2001).

[58] The implementation details of the nonequilibrium Green's-function-based DFT technique can be found elsewhere [Jeremy Taylor, Ph.D. thesis, McGill University (2000); Jeremy Taylor, Hong Guo, and J. Wang, Phys. Rev. B **63**, 245407 (2001).

[59] K. Raghavachari and J. S. Binkley, J. Chem. Phys. **87**, 2191 (1987).

[60] A. P. Jauho, N. S. Wingreen, and Y. Meir, Phys. Rev. B **50**, 5528 (1994).

[61] S. Datta, *Electronic Transport in Mesoscopic Systems* (Cambridge University Press, New York, 1995).

[62] B. G. Wang, J. Wang, and Hong Guo, Phys. Rev. Lett. **82**, 398 (1999); J. Appl. Phys. **86**, 5094 (1999).

[63] P. Ordejón, E. Artacho, and José M. Soler, Phys. Rev. B **53**, R10 441 (1996).

[64] D. R. Hamann, M. Schlüter, and C. Chiang, Phys. Rev. Lett. **43**, 1494 (1982).

[65] G. Taraschi, M.Sc. thesis, McGill University (1997).

[66] O. F. Sankey and D. J. Niklewski, Phys. Rev. B **40**, 3979 (1989).

[67] S. Sanvito, C. J. Lambert, J. H. Jefferson, and A. M. Bratkovsky, Phys. Rev. B **59**, 11 936 (1999).

[68] See, for example, articles in *Nanostructures and Mesoscopic Systems*, edited by Wiley P. Kirk and Mark A. Reed (Academic Press, Boston, 1992).

[69] In Figs. 4(a) and 4(b) the transmission coefficient $T(E)$ has two large peak structures with $T \sim 2$. The position of these peaks correspond to the HOMO and LUMO energies of the carbon chains. There are other resonances at lower energy (did not show) that correspond to lower molecular orbitals. $T(E)$ is also affected by the electrode band gaps, which give rise to the other sharp structures on the curve of $T(E)$. For example, for the even chain, Fig. 4(a) shows that the LUMO (solid triangle) seems to not align exactly to the $T(E)$ peak, but to the right of it. This is because the LUMO energy happens to fall into an electrode band gap in which there is no transmission. Therefore before $T(E)$ develops a peak exactly at LUMO, it drops down to very small values as shown in Fig. 4(a).

[70] When d is varied, both electrode-chain contact distances are varied by the same amount.

[71] The amount of charge transferred to the chain is almost entirely due to the chain-electrode contact distance d. In the complete range of bias voltage ΔV that we have investigated, the charge transfer difference is $<1\%$.